Werk

Jahr: 1988
Kollektion: fid.geo
Signatur: 8 Z NAT 2148:62
Digitalisiert: Niedersächsische Staats- und Universitätsbibliothek Göttingen
Werk Id: PPN1015067948_0062
PURL: http://resolver.sub.uni-goettingen.de/purl?PPN1015067948_0062

LOG Id: LOG_0032
LOG Titel: Restoration of broad-band seismograms (Part II): Signal moment determination
LOG Typ: article

Übergeordnetes Werk

Werk Id: PPN1015067948
PURL: http://resolver.sub.uni-goettingen.de/purl?PPN1015067948
OPAC: http://opac.sub.uni-goettingen.de/DB=1/PPN?PPN=1015067948

Contact

Niedersächsische Staats- und Universitätsbibliothek Göttingen
Georg-August-Universität Göttingen
Platz der Göttinger Sieben 1
37073 Göttingen
Germany
Email: gdz@sub.uni-goettingen.de

J Geophys (1988) 62:158–162

Journal of Geophysics

Restoration of broad-band seismograms (Part II): Signal moment determination

D. Seidl[1] and M. Hellweg[2]

[1] Seismologisches Zentralobservatorium Gräfenberg, Krankenhausstr. 1, D-8520 Erlangen, Federal Republic of Germany
[2] 57 Overhill Road, Orinda, CA 94563-3122, U.S.A.

Abstract. Two standard methods for the time-domain determination of the signal moment from displacement seismograms are studied theoretically and numerically using broad-band data. Investigation shows that the accuracy of the displacement integral method depends relatively little on the shape of the body-wave displacement pulse, but strongly on the ratio of the pulse duration d to the seismometer period T_0. For a single-sided wavelet of duration d, the signal moment can be determined with a relative error $\langle e$ if the seismometer period $T_0 \rangle 2\pi d/e$. The displacement impulse method for wavelets with corner frequencies greater than the cut-off frequency of the seismograph is discussed for the broad-band channel of the Gräfenberg array. The theoretical results are illustrated using broad-band recordings of the Gräfenberg array.

Key words: Source moment – Displacement integral – Displacement impulse – Broad-band seismograms – Restoration

Introduction

The inversion of displacement waveforms is the basis for the determination of source parameters such as focal depth, fault-plane parameters and moment. The wider the bandwidth of the recording, the more accurate the seismic interpretation can be. The Wielandt-Streckeisen broad-band seismometer (Wielandt and Streckeisen, 1982), which records ground motion as velocity or displacement from 0.2 s to 20 s, and the improved Wielandt-Steim very broad-band version (Wielandt and Steim, 1986), with an upper corner period of 360 s, produce such wide-band recordings. The characteristic properties of digital broad-band seismographs – low seismometer noise, an exact transfer function, high linearity, large bandwidth and high dynamic range – allow the upper corner period to be increased still further numerically. In addition, velocity seismograms can easily be converted to displacement seismograms.

With the advent of broad-band digital seismographs, the accuracy and resolution of signal parameters used in source studies can be improved using wide-band restoration. Restoration of broad-band seismograms Part I (Seidl and Stammler, 1984) discussed the seismograph characteristics of the Gräfenberg array in the time and frequency domains, various methods for the computation of synthetic seismograms and the instrumental correction for the measurement of arrival times and first-motion signs. Part II addresses the problem of wide-band restoration and the determination of signal moment.

Offprint requests to: D. Seidl

Signal moment determination

The source moment M_0 can be calculated from the P- or S-wave signal moment

$$m_u = \int_0^\infty u(t)\,dt = \bar{U}(0), \tag{1}$$

using the expression

$$M_0 = G \cdot m_u. \tag{2}$$

$u(t)$ is the displacement wavelet [$u(t)=0$ for $t<0$] of the P or S wave and $\bar{U}(0)$ is its spectral value at frequency zero. G corrects for the radiation pattern of the source, the geometrical amplitude spreading and the attenuation factor of the propagation path.

If $u(t)$ is recorded by a seismograph with the frequency characteristics $\bar{H}(j\omega)$, the spectrum $\bar{S}(j\omega)$ of the seismogram $\bar{s}(t)$ has the form

$$\bar{S}(j\omega) = \int_0^\infty \bar{s}(t) \exp(-j\omega t)\,dt = \bar{U}(j\omega) \cdot \bar{H}(j\omega). \tag{3}$$

The seismogram moment m_s, obtained from Eq. (3) for $\omega = 0$, is

$$m_s = \int_0^\infty \bar{s}(t)\,dt = \bar{U}(0) \cdot \bar{H}(0) = 0 \tag{4}$$

since $\bar{H}(0)=0$ for seismometers with mechanical pendulum sensors.

The approximate signal moment m_u is usually estimated in the frequency domain by the sequence of operations: Selection of a seismogram window → Fourier transform $\bar{S}(j\omega)$ → instrument correction $\bar{U}(j\omega) = \bar{S}(j\omega)/\bar{H}(j\omega)$ → extrapolation of the "low-frequency plateau range" of $|\bar{U}(j\omega)|$ to frequency zero.

In the time domain, the moment can be approximated using the displacement integral with a finite upper limit t_0. This finite integral corresponds to the extrapolation of the displacement spectrum into the frequency interval $\{0, 1/t_0\}$. The displacement time function for the integration must be determined by restoration from a recorded velocity or displacement seismogram. In this case, restoration means increasing the seismometer period using numerical methods

until the seismogram becomes unstable due to the long-period noise.

For a small signal-to-noise ratio, a sufficient base-line correction cannot be performed by linear trend removal and high-pass filtering. In this case, analysis in the time domain has an advantage over the frequency domain because the instantaneous low-frequency trend of the seismogram can be used as the time axis for the computation of the displacement integral. Such a correction for the low-frequency noise is not possible in the frequency domain.

The displacement integral method

To a certain extent, the effects of signal shape, seismometer frequency and integration interval on the accuracy of the signal moment determination can be investigated theoretically. The far-field displacement P or S waveform for a unilateral rupture with finite fault length and finite slip function rise time is a single-sided wavelet with a spectrum proportional to ω^{-2} for high frequencies. The time function

$$u(t)=m_u\cdot a^2\cdot t\cdot\exp(-a\cdot t)\cdot\bar{h}(t), \tag{5}$$

where $\bar{h}(t)$ is the unit step response, can be used as an analytically simple signal model for such a displacement pulse with the moment m_u. A practical definition of the signal duration d is the time within which the signal decays to about 0.7% to the maximum amplitude:

$$d=\frac{8}{a}. \tag{6}$$

The wavelet in Eq. (5) has the Laplace transform

$$U(s)=\frac{m_u\cdot a^2}{(s+a)^2} \tag{7}$$

and the Fourier transform $\bar{U}(j\omega)=U(s)|_{s=j\omega}$. The wavelet spectrum $|\bar{U}(j\omega)|$ is a negative monotonic function with the upper corner frequency

$$f_c=\frac{\sqrt{\sqrt{2}-1}}{2\cdot\pi}\cdot a\approx 0.1024\cdot a \tag{8}$$

and a spectral fall-off $\sim\omega^{-2}$ for high frequencies.

For a displacement seismometer with critical damping, angular eigenfrequency ω_0 and the transfer function

$$H(s)=\frac{s^2}{(s+\omega_0)^2}, \tag{9}$$

the response $\bar{s}(t)$ to the input wavelet in Eq. (5) is obtained by evaluating the inverse Laplace transform of the rational function $U(s)\,H(s)$:

$$\bar{s}(t)=m_u\cdot a^2\left\{\left[\frac{\omega_0^2\cdot t}{(a-\omega_0)^2}-\frac{2\cdot a\cdot\omega_0}{(a-\omega_0)^3}\right]\exp(-\omega_0\cdot t)+\left[\frac{a_0^2\cdot t}{(a-\omega_0)^2}-\frac{2\cdot a\cdot\omega_0}{(a-\omega_0)^3}\right]\exp(-a\cdot t)\right\}. \tag{10}$$

In the special case $a=\omega_0$, Eq. (10) becomes indeterminate. However, $\bar{s}(t)$ can still be described analytically using L'Hospital's rule:

$$\bar{s}(t)=m_u\left(t-\omega_0 t^2+\frac{\omega_0^2}{6}t^3\right)\exp(-\omega_0 t). \tag{11}$$

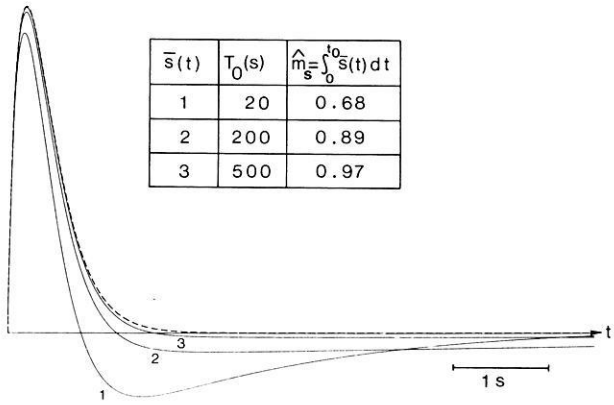

Fig. 1. Theoretical seismograms for two broad-band (*solid lines* 1 *and* 2) and one very broad-band (*solid line* 3) displacement seismographs (period T_0) for the displacement wavelet $u(t)=m_u\cdot a^2\cdot t\exp(-a\cdot t)$ (*dashed line*) with moment $m_u=1$. a has the value 4.88 s^{-1} corresponding to an upper corner frequency of $f_c=0.5$ Hz. The apparent seismogram moment $\hat{m}_s=\int_0^{t_0}\bar{s}(t)\,dt$ (t_0 time of zero crossing) tends to the input moment $m_u=1$ for $T_0\to\infty$

Equation (10) shows that the seismogram $\bar{s}(t)$ approaches the input wavelet $u(t)$ if the seismometer frequency ω_0 tends to zero:

$$\lim_{\omega_0\to 0}\bar{s}(t)=m_u\cdot a^2\cdot t\cdot\exp(-a\cdot t). \tag{12}$$

In Fig. 1 the theoretical seismograms calculated using Eq. (10) approach the input wavelet when the seismometer period T_0 is increased. Since $\int_0^{\infty}\bar{s}(t)\,dt=0$ [Eq. (4)], the seismogram $\bar{s}(t)$ crosses zero at least once at t_0 and overshoots for any finite seismometer period. The finite displacement integral $\int_0^{t_0}\bar{s}(t)\,dt$ will be called the apparent seismogram moment $\hat{m}_s$. Hence, the moment m_u of the input wavelet can be written as follows:

$$m_u=\int_0^{t_0}\bar{s}(t)\,dt+e(f_c, T_0). \tag{13}$$

Equation (13) is illustrated in Fig. 1. For a wavelet with a time function described by Eq. (5) and upper corner frequency as in Eq. (8), and given an error $e>0$, there exists a seismometer period T_0' such that $|m_u-\hat{m}_s|<e$ for $T_0>T_0'$.

How does the error term in Eq. (13) depend on the shape of the input wavelet? The response of the seismometer in Eq. (9) to a rectangular wavelet of duration d and moment m_u

$$u(t)=\frac{m_u}{d}[\bar{h}(t)-\bar{h}(t-d)] \tag{14}$$

is given by

$$\bar{s}(t)=\frac{m_u}{d}\{(1-\omega_0 t)\exp(-\omega_0 t)\,\bar{h}(t)-[(1-\omega_0(t-d))\cdot\exp(-\omega_0(t-d))]\,\bar{h}(t-d)\}.$$

As in Eq. (12), the seismogram tends to the input wavelet in Eq. (14) for the limit $\omega_0\to 0$.

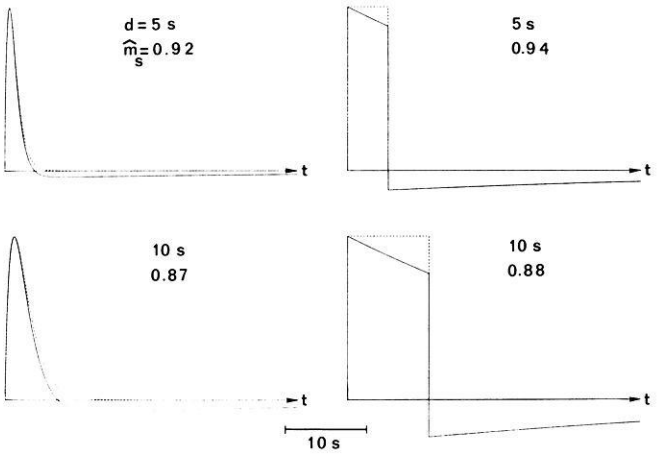

Fig. 2. Apparent moment and wavelet shape: theoretical seismograms (*solid lines*) and apparent moments $\hat{m}_s$ for a very broad-band seismograph ($T_0 = 500$ s) for the exponential [Eq. (5), *left*] and rectangular [Eq. (14), *right*] input wavelet (duration d). $\hat{m}_s$ has nearly the same value for both wavelets

Linearizing Eq. (15) for $\omega_0 \cdot t \ll 1$ and integrating over the interval d gives an approximation for the apparent moment

$$\hat{m}_s = m_u \cdot (1 - \omega_0 \cdot d). \tag{16}$$

The relative error is then $e = (\hat{m}_s - m_u)/m_u = -\omega_0 \cdot d$.

Figure 2 shows that $\hat{m}_s$ has nearly the same value for the exponential wavelet in Eq. (5) and for the rectangular wavelet in Eq. (14). A similar result is obtained for a half-cycle sinusoidal pulse. Since the spectra of single-sided time functions are all negatively monotonic and flat near frequency zero, $\hat{m}_s$ depends only weakly on the shape of the input wavelet.

Figure 3 shows a diagram of the apparent moment $\hat{m}_s$ versus the duration d for an exponential and a rectangular wavelet and for displacement seismometers with different periods. The straight lines defined by Eq. (16) satisfactorily approximate both curves for $\omega_0 \cdot d \ll 1$. As a rule of thumb, the relative error is less than about 10% if the seismometer period $T_0 > 20\pi d$ [Eq. (16)]. For a very broad-band seismometer ($T_0 = 360$ s) the relative error is therefore less than 10% for pulse durations up to about 6 s.

The displacement impulse method

If the upper corner frequency of the displacement wavelet is greater than the cut-off frequency of the seismograph, the seismogram $\bar{s}(t)$ has approximately the form $\bar{s}(t) \approx m_u \cdot h(t)$, where $h(t)$ is the displacement impulse response of the seismograph and m_u is the moment of the input wavelet. This approximation follows from the series representation of the seismogram in terms of the derivatives $h^{(k)}(t)$ and the moments

$$m_{uk} = \int_0^\infty t^k u(t)\, dt \qquad k = 0, 1, 2, \ldots \tag{17}$$

of the input wavelet (see, for example, Papoulis, 1977):

$$\bar{s}(t) = \sum_{k=0}^{\infty} (-1)^k \cdot m_{uk} \cdot h^{(k)}(t) = m_u \cdot h(t) + m_{u1} \cdot h'(t) + \ldots \tag{18}$$

with $m_{u0} = m_u$.

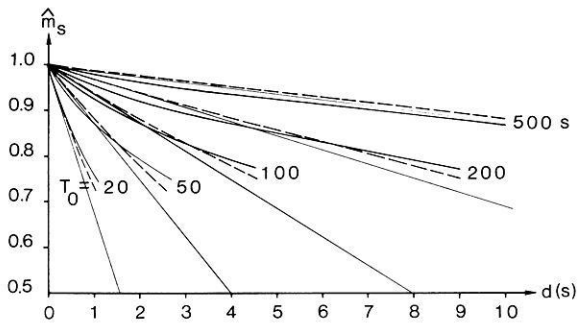

Fig. 3. Apparent seismogram moment $\hat{m}_s$ versus duration d for two input wavelets with moment $m_u = 1$ (*solid curves* – exponential wavelet; *dashed curves* – rectangular wavelet) for displacement seismographs with periods T_0. The *straight lines* $\hat{m}_s = m_u \cdot (1 - \omega_0 d)$ of Eq. (16) approximate both curves for $\omega_0 \cdot d \ll 1$, where $\omega_0 = 2\pi/T_0$ is the angular eigenfrequency of the seismometer

Inserting the exponential wavelet in Eq. (5) into Eq. (17), it follows

$$m_{uk} = m_u \cdot a^2 \cdot \int_0^\infty t^{k+1} \cdot \exp(-a \cdot t)\, dt = m_u \cdot \frac{(k+1)!}{a^k}. \tag{19}$$

Expressing a in terms of the wavelet duration in Eq. (6), Eq. (19) can be written as

$$m_{uk} = m_u \frac{(k+1)!}{8^k} d^k. \tag{20}$$

Substituting Eq. (20) into Eq. (18) gives

$$\bar{s}(t) = m_u \sum_{k=0}^{\infty} \frac{(-1)^k \cdot (k+1)!}{8^k} \cdot h^{(k)}(t) \cdot d^k$$

$$= m_u \left[h(t) - \frac{1}{4} h'(t) \cdot d + \frac{3}{32} h''(t) \cdot d^2 + \ldots \right]. \tag{21}$$

Hence, for small duration d of the input wavelet, the seismogram is approximately given by the first term in the expansion $m_u \cdot h(t)$. For the broad-band velocity channel of the Gräfenberg array, the range of pulse durations for which this approximation is valid is shown in Fig. 4. The theoretical seismograms are calculated using the impulse invariant transformation (Seidl and Stammler, 1984). For upper corner frequencies of the exponential wavelet $f_c \geqq 5$ Hz, the seismograms can be described by the function $b(f_c) \cdot m_u \cdot \tilde{h}(t)$, where $b(f_c)$ is the maximum amplitude of the synthetic response in terms of the corner frequency f_c. $b(f_c)$ decreases very slowly from $b = 1.0$ for high frequencies to $b = 0.86$ for $f_c = 5$ Hz (cut-off frequency of the Gräfenberg seismograph) and $\tilde{h}(t)$ has nearly the same shape as the impulse response $h(t)$. For $f_c < 5$ Hz, $b(f_c)$ decreases very rapidly (for example, $b = 0.2$ for $f_c = 2$ Hz) and the seismogram shows increasing deviation from the impulse response. This sharp transition is caused by the steep slope of 36 dB per octave of the amplitude response of the Gräfenberg velocity channel. Thus, the influence of a change in moment on the observed pulse amplitude can be separated from the effects of a change in the corner frequency. The usually steep fall-off generated by the anti-aliasing filter of a digital seismograph is therefore very useful for the application of the displacement impulse method.

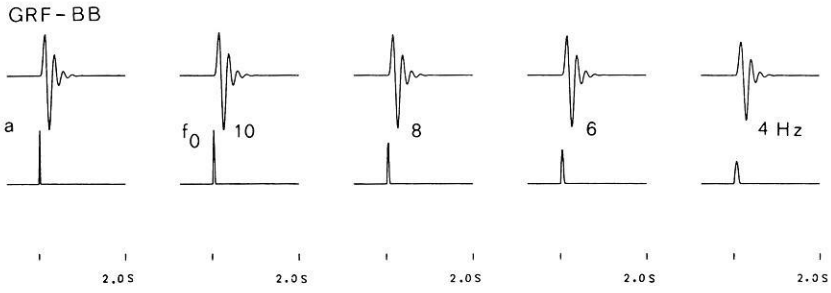

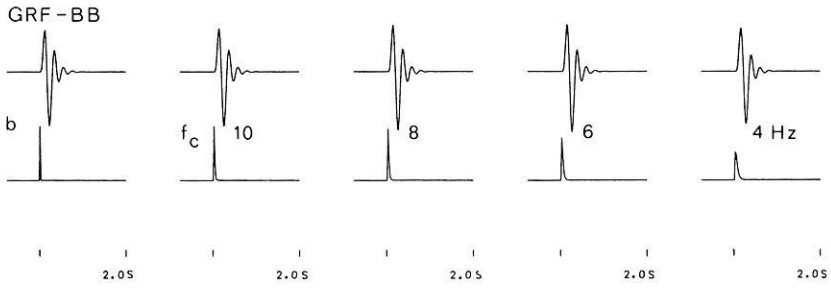

Fig. 4a and b. Synthetic seismograms for the broad-band velocity channel of the Gräfenberg array for **a** a half-cycle sinusoidal wavelet with frequency f_0 and **b** the exponential wavelet from Eq. (5) with corner frequency f_c. In both cases the first seismogram is the displacement impulse response. The input wavelets are normalized to the moment $m_u = 1$

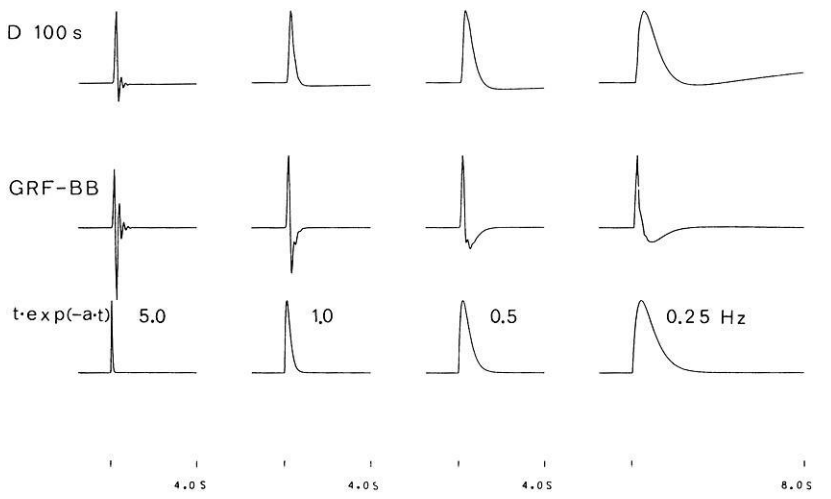

Fig. 5. Restoration of synthetic seismograms. *Bottom*: exponential displacement wavelets with various corner frequencies normalized to the maximum amplitude. *Middle*: the corresponding synthetic seismograms for the Gräfenberg velocity channel (GRF-BB). *Top*: restoration of the GRF-BB synthetic seismograms for a displacement seismograph ($T_0 = 100$ s) including the Gräfenberg anti-aliasing filter

In contrast, the transition in $b(f_c)$ and $h(t)$ for the standard narrow-band seismographs with a flatter high-frequency fall-off is more gradual. The separation of moment and corner frequency effects at intermediate frequencies is therefore not as easy. For example, Randall (1972) has described the method using WWSSN-LP seismograms.

The most important application of the displacement impulse method is the moment estimation for local events, especially the determination of relative moments for shock sequences.

Restoration of broad-band seismograms

Restoration is the approximate reconstruction of the true ground motion from the seismogram. One possible procedure is performed for a displacement seismograph by shifting the seismometer period to higher values. The long-period boundary is limited mainly by the low-frequency noise. For a velocity seismograph, an additional integration is necessary. For small signal-to-noise ratio, a base-line correction should be performed by linear trend removal and high-pass filtering. Of the many well-known procedures, a practical time-domain method is increasing the seismometer period stepwise and integration for velocity seismograms until the seismogram form remains nearly unchanged or the seismogram becomes unstable due to amplified low-frequency noise.

Figure 5 uses synthetic seismograms to demonstrate restoration. The high-quality result is due to the lack of noise in the original seismograms. The deviations are caused by the anti-aliasing filter and the overshoot effect described in Eq. (4). The synthetic and restored signals are calculated using the impulse invariant transformation (Seidl and Stammler, 1984).

Practical examples

Figure 6 shows the time-domain restoration for the Gräfenberg velocity recording of a teleseismic *P* wave. The restoration was performed using a recursive simulation filter for a seismometer-galvanometer system with amplitude characteristics proportional to displacement in the period band from 0.2 s to the indicated upper period (Seidl, 1980). Overshooting in the displacement seismograms decreases with increasing upper period, in good agreement with Eq. (10), indicating a single-sided *P* wavelet. For upper periods

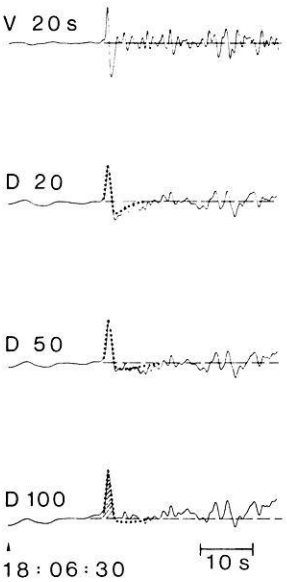

Fig. 6. Gräfenberg broad-band velocity recording (V) of a teleseismic P wavegroup and the restored displacement seismograms (D) for increasing seismograph period. Notice the decrease in overshoot with increasing period. The *dots* indicate the synthetic seismograms of Eq. (10).
Station GRF-A1Z, epicentral distance 84°, Honshu 09/24/1980, $mb = 6.0$, depth = 73 km. Apparent seismogram moment of the P pulse (*shaded area*) $\hat{m}_s = 0.32 \times 10^{-5}$ m·s

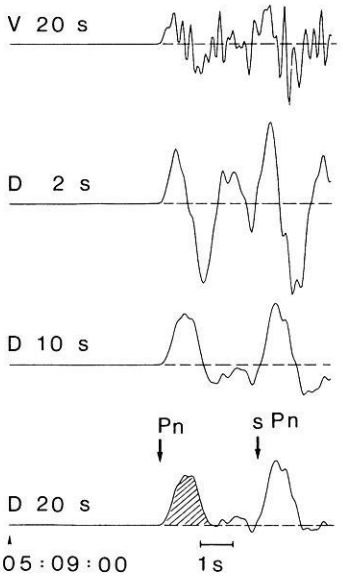

Fig. 7. Gräfenberg broad-band velocity recording (V) of a short-period local $Pn-sPn$ wavegroup and the restored displacement seismograms (D) for increasing seismograph period.
Station GRF-A1Z, epicentral distance 220 km, Swabian Jura 09/03/1978, $MS = 5.5$, depth = 6.5 km. Apparent seismogram moment of the Pn pulse (*shaded area*) $\hat{m}_s = 6.2 \times 10^{-6}$ m·s. Source moment $M_0 = 0.34 \times 10^{17}$ Nm (Haessler et al., 1980)

greater than 100.0 s, the overshooting is less than the noise level. The signal duration is about 2.5 s and the relative error of the apparent moment is about 15%.

Figure 7 shows the restoration of a $Pn-sPn$ wavegroup, using the procedure described for Fig. 6. For an upper period $T_0 = 20.0$ s, a nearly single-sided pulse of about 1.5 s duration is obtained. The overshooting is less than for the synthetic seismogram 1 in Fig. 1, calculated for a seismometer period $T_0 = 20.0$ s and a pulse duration $d = 1.6$ s. This indicates that the P pulse is a composite and/or non-single-sided wavelet. The apparent moment should therefore be used with caution for the determination of the source moment by applying standard geometric P-wave spreading factors. In this case, waveform inversion using theoretical seismograms should be preferred to estimate the source moment.

Conclusions

The moment of a single-sided wavelet can be determined from a broad-band displacement seismogram using a finite displacement integral. Velocity recordings must first be converted to displacement seismograms by a wide-band restoration procedure. The relative error of the seismogram moment depends mainly on the ratio of the seismogram wavelet duration to the upper period of the seismograph. An advantage of this time-domain method is the ability to correct for long-period noise in the wideband displacement seismograms.

If the upper corner frequency of a wavelet is greater than the cut-off frequency of the seismograph, the seismogram is nearly the impulse response of the seismograph. In this case, the moment can be estimated from the maximum seismogram amplitude. The frequency range for the valid application of this method can be determined using synthetic seismograms.

Correctly applied, these methods may improve the accuracy of signal moment determination. Although the corrections are small compared to the uncertainties due to path and radiation effects, they may reduce scatter in moment vs. energy or moment vs. magnitude curves studied in shock sequences.

Acknowledgements. This paper was part of a joint project of the Institute for Meteorology and Geophysics of the University of Frankfurt and the Central Seismological Observatory Gräfenberg, supported by the German Research Council. We would like to thank E. Wielandt for many detailed comments, especially for discovering Eq. (16). The Gräfenberg array is part of the Bundesanstalt für Geowissenschaften und Rohstoffe (Federal Institute for Geosciences and Natural Resources) and is supported by the Deutsche Forschungsgemeinschaft (German Research Council).

References

Haessler, H., Hoang-Trong, P., Schick, R., Schneider, G., Strohbach, K.: The September 3, 1978, Swabian Jura earthquake. Tectonophysics **68**, 1–14, 1980

Papoulis, A.: Signal analysis, pp. 102–104. McGraw-Hill 1977

Randall, M.J.: Multipolar analysis of the mechanisms of deep-focus earthquakes. In: Methods in computational physics, Vol. 12, pp. 280–283. New York and London: Academic Press 1972

Seidl, D.: The simulation problem for broad-band seismograms. J. Geophys. **48**, 84–93, 1980

Seidl, D., Stammler, W.: Restoration of broad-band seismograms (Part I). J. Geophys. **54**, 114–122, 1984

Wielandt, E., Steim, J.M.: A digital very-broad-band seismograph. Ann. Géophys. **4**, 227–232, 1986

Wielandt, E.: Streckeisen, G.: The leaf-spring seismometer. Design and performance. Bull. Seismol. Soc. Am. **72**, 2349–2367, 1982

Received September 2, 1987; revised version October 26, 1987
Accepted October 27, 1987